Study of ground vibration induced by high-speed trains moving on multi-span bridges

S.H. Ju[*]

Department of Civil Engineering, National Cheng-Kung University, Tainan City, Taiwan, R.O.C.

Abstract. This paper investigates the ground vibration induced by high-speed trains moving on multi-span continuous bridges. The dynamic impact factor of multi-span continuous bridges under trainloads was first determined in the parametric study, which shows that the dynamic impact factor will be large when the first bridge vertical natural frequency is equal to the trainload dominant frequencies, nV/D, where n is a positive integer, V is the train speed, and D is the train carriage interval. In addition, more continuous spans will produce smaller dynamic impact factors at this resonance condition. Based on the results of three-dimensional finite element analyses using the soil-structure interaction for realistic high-speed railway bridges, we suggest that the bridge span be set at 1.4 to 1.5 times the carriage interval for simply supported bridges. If not, the use of four or more-than-four-span continuous bridges is suggested to reduce the train-induced vibration. This study also indicates that the vibration in the train is major generated from the rail irregularities and that from the bridge deformation is not dominant.

Keywords: finite element analysis; high-speed train; impact factor; multi-span bridge; resonance; trainload dominant frequency; vibration

1. Introduction

Moving high-speed trains often produce significant ground vibration, which may produce environmental problems, as well as making things uncomfortable for passengers. Thus, designing an optimal railway system to reduce train induced vibration is an increasingly important task. Yang *et al*. (1997) examined the vibration of simple beams subjected to the passage of trainloads. Based on the conditions of resonance and cancellation for the waves generated by continuously moving loads on the beam, a set of optimal design criteria were proposed that are effective in suppressing the resonant responses. Wang *et al*. (2010) investigated the resonance of a two-span continuous bridge under moving trainloads, and found that inclusion of beam damping can help in reducing the train-induced resonant beam response. Several researchers have reported that the bridge slabs, rails, or sleepers can be modified to reduce train-induced vibration (Ju 2004, Kim *et al*. 2004, Xia *et al*. 2010, Xin and Gao 2011), while a number of studies used suitable dampers to reduce the bridge vibration induced by moving trains (Museros *et al*. 2007, Wang *et al*. 2013, Fiebig 2010, Lavado *et al*. 2014), Alternatively, some researchers changed the bridge sections or the train speed

---

∗Corresponding author, Professor, E-mail: juju@mail.ncku.edu.tw

to avoid resonance between bridges and trainloads, as this can also reduce the vibration induced by a moving train (Ju 2002, Yang *et al.* 2004, Kim and Kim 2010, Kwark 2012, Mao and Lu 2013, Arvidsson 2014, Adam and Salcher 2014, Aflatooni 2015),

A multi-span continuous bridge is an appropriate structure for use with a high-speed railway system. However, not many researchers have investigated the vibration induced by this type of bridge, and few studies have applied three-dimensional (3D) analysis to investigate the realistic behavior of train-induced vibration. This paper first uses a continuous beam analysis to study the resonance behavior of trains and bridges, and 3D nonlinear finite element analyses with a large degrees of freedom are then performed to study the advantages of multi-span bridges.

2. Dynamic impact factor of multi-span continuous bridges for train loads

This section evaluates the dynamic impact factor of multi-span continuous bridges for train loads to study the vibration behavior of such structures. The bridge is an *N*-span (*N*=1 to 5 and 12) continuous beam with the equal span length (*L*) of 30 m, where the leftmost and rightmost sides are simply supported and the other *N*-1 supports are rollers in the vertical direction. The beam properties are the same as the standard bridge section of the Taiwan high-speed rail system, where the first vertical natural frequencies of the *N*-span continuous bridges are the same and equal to 4.641 Hz. The train loads are 12 equal concentrated loads with an equal space *D* under a constant train speed *V*, in which *D* and *V* will be set as variables in the parametric study. The average dynamic impact factor is defined as follows

$$I = \frac{1}{N} \sum_{i=1}^{N} \frac{R_d(x_i)}{R_s(x_i)} \tag{1}$$

where $R_d(x_i)$ *and* $R_s(x_i)$ are the maximum dynamic and static displacements in the vertical direction at the ith midpoint of the *N*-span continuous beams due to the action of the moving loads, respectively.

In the parametric study, we follow Yang *et al.* (1997) and set the damping of the bridge to zero. The train speed (*V*) is set from 20 m/s to 200 m/s, at intervals of 5 m/s, and the load interval (*D*) is set from 17 m to 51 m, at intervals of 2 m. The finite element method with the Newmark integration method is used to find the bridge's static and dynamic responses, and the dynamic impact factors are then determined. The 2-node beam element with the length of 1 m is used, the time step length is set to 0.001 s, and the consistent mass scheme is used. Wireframe figures for 1- to 5- and 12-span continuous beams are plotted in Fig. 1, where the horizontal *X* axis (Bridge_Freq/(*V/D*)) is the first vertical bridge natural frequency divided by the train speed (*V*) over the load interval (*D*), the horizontal *Y* axis (*L/D*) is the bridge length between two supports (*L*) divided by the train interval (*D*), and the vertical axis is the dynamic impact factor (*I*) of equation (1). Fig. 1 indicates the following features:

(1) For all the bridge types in Fig. 1, the dynamic impact factor will be large when the first bridge vertical natural frequency is equal to *nV/D*, where *n* is 1, 2, 3, …, a positive integer, and this condition is especially obvious for *n*=1. Yang *et al.* (1997) stated this resonance condition for simply supported bridges. Ju *et al.* (2009) used field experiments and train load formulations to prove that the train-induced vibration will be larger at the train's dominant frequency (*nV/D*) both for trains moving on bridges and embankments, and a resonance occurs
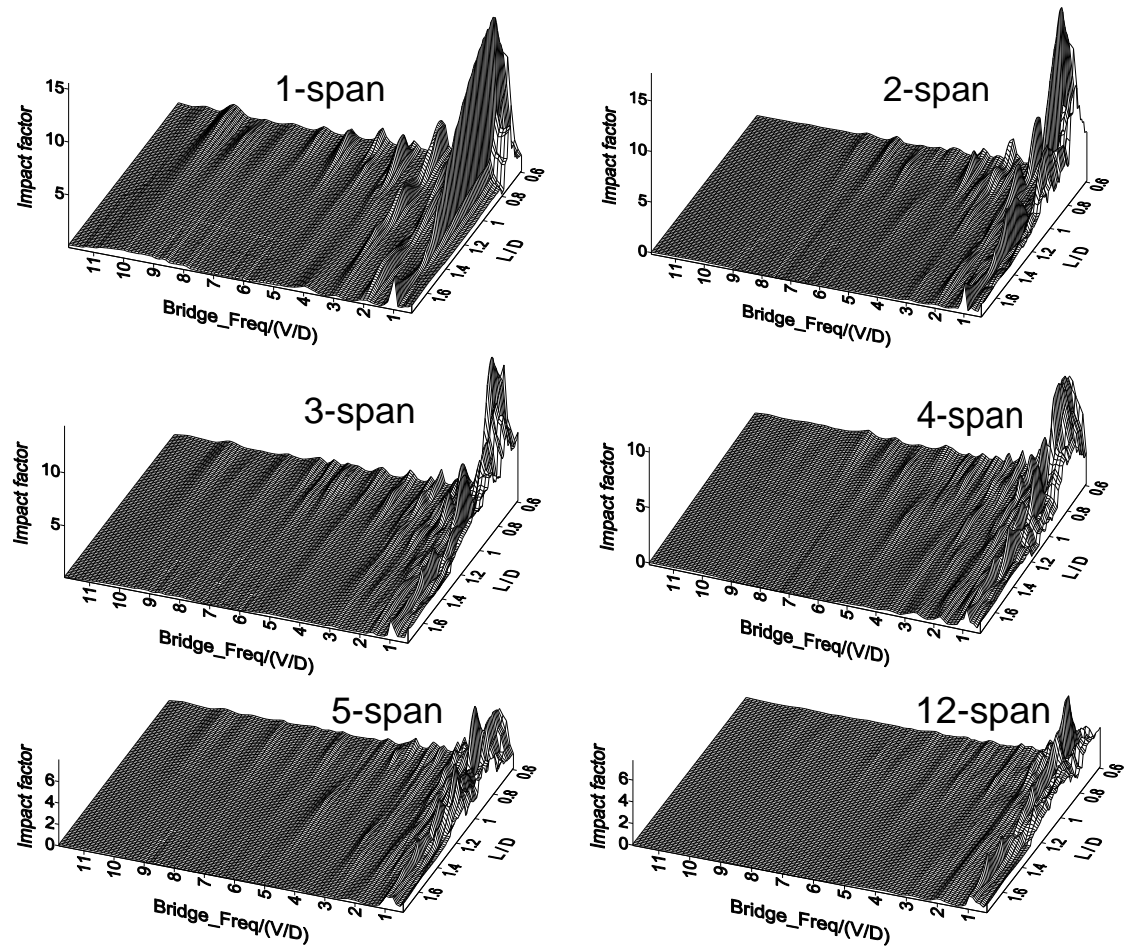
Fig. 1 Wireframe figures of the dynamic impact factor changing with bridge span length over the load interval (L/D) and bridge natural frequency over the train speed/load interval (Bridge_Freq/(V/D)) for six types of continuous bridges

when the train dominant frequencies are equal to the bridge's natural frequency. These conclusions are exactly the same as the effects shown in Fig. 1.

(2) The resonance is more serious for a smaller ratio of *L/D*. If the trainload interval (*D*) is constant, a shorter beam support interval (*L*) will produce a larger vibration when resonance occurs. This condition should be avoided when designing a bridge system for moving trains. The first vertical natural frequency of a bridge for high-speed trains is usually much larger than the first dominant frequency (*V/D*) of the trainload, and a shorter support interval can make the difference even larger, so it is almost impossible to achieve resonance between the first trainload dominant frequency and the first bridge vertical natural frequency. However, the resonance of the second and third trainload dominant frequencies and the first bridge vertical natural frequency usually cannot be avoided.

(3) Comparing with the vertical axis range of each plot in Fig. 1, one can conclude that more continuous spans will produce smaller dynamic impact factors at the resonance conditions. This

can be explained by the moment influence line at the mid-span of the continuous beam, where the adjacent spans of the mid-span will have a negative sign of the influence line compared to that of the mid-span, so that the trainloads passing the adjacent span will reduce the vibration at the mid-span. In practice, it is difficult to build bridges with a large number of continuous spans, since the changes in temperature may cause mechanical problems. However, the use of four or five continuous spans is still very acceptable for bridge systems.

(4) For the simply supported beam under L/D around 1.4 to 1.5, the dynamic impact factor can be minimized for the resonance of the first trainload and the first bridge natural frequency, and this condition was first noted by Yang *et al.* (1997), However, the resonance between the second or third dominant frequencies and the first bridge natural frequency still cannot be avoided. For other types of continuous bridges, an L/D over 1.2 will generally not cause a large dynamic impact factor.

This section uses continuous beam analyses to study the vibration behavior of multi-span continuous bridges under moving loads. The conditions will be more complicated for realistic high-speed rail bridges, so the 3D finite element method will be used to investigate the train-induce ground vibration for multi-span continuous bridges in the following sections.

3. Finite element formulation and model for analysis of train-induced vibration

3.1 Finite element formulation

The studied high-speed train is the SKS-700 type with 12 carriages, 24 bogies and 48 wheel sets moving in the X direction, while a 3D model for this train can be found in the literature (Ju 2013), and this section will briefly explain the elements. The vertical direction is in the Z direction and the Y direction is perpendicular to the railway. For the moving wheel element, the three-node element stiffness for the nodal displacements (d_1, θ_1, d_2, d_3, θ_3) is

$$\mathbf{S} = \mathbf{T}^T \begin{bmatrix} k_r & -k_r \\ -k_r & k_r \end{bmatrix} \mathbf{T}, \quad T = \begin{bmatrix} 0 & 0 & 1 & 0 & 0 \\ N_1 & N_2 & 0 & N_3 & N_4 \end{bmatrix} \quad (2)$$

where d_1, θ_1, d_3 and θ_3 are the translations and rotations at target nodes 1 and 3, d_2 is the translation of the wheel node, N_i=the cubic Hermitian interpolation functions, and k_r is the stiffness between the rail and wheel. In the horizontal (Y) direction, k_r is a constant of 4.3×10^4 KN/m for the contact of the JIS-60 rail and SKS-700 wheel. In the vertical (Z) direction, k_r is approximately a power function of $k_r = a + bf_2^c$, where a=3×10^4 KN/m, b=2.5×10^5 KN/m, c=0.254, and f_2 is the contact force (KN) between the wheel and rail. The internal force vector of the wheel element is

$$\begin{bmatrix} f_1 & m_1 & f_2 & f_3 & m_3 \end{bmatrix}^T = \mathbf{S} \begin{bmatrix} d_1 & \theta_1 & d_2 & d_3 & \theta_3 \end{bmatrix}^T - \begin{bmatrix} N_1 & N_2 & -1 & N_3 & N_4 \end{bmatrix} k_r r_v(X) \quad (3)$$

where (f_1, m_1, f_2, f_3, m_3) are internal forces and moments at nodes 1, 2 and 3, and the nodal forces should exclude the terms of rail irregularities $r_v(X)$. In this paper, the formulation and input data of $r_v(X)$ is obtained from (Ju 2012). For the contact force f_2, if it is negative, the wheel and rail are in contact together. Otherwise, they are separated, and k_r is set at zero for the next Newton-Raphson iteration. For a spring or damper connected to two master nodes, the stiffness or damping matrix is
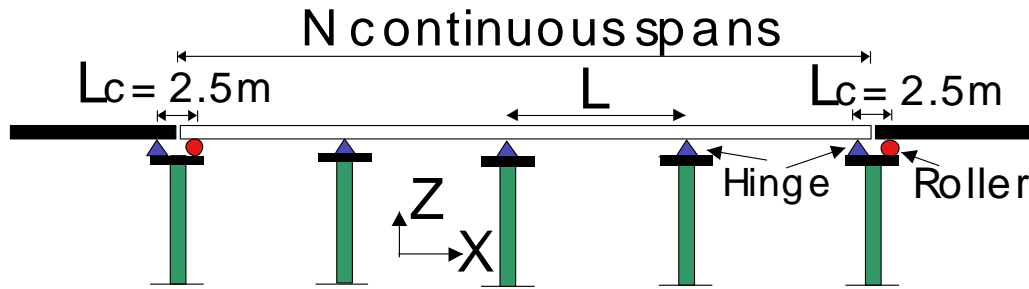
Fig. 2 Illustration of the multi-span bridge structure

$$\mathbf{S} = s\,\mathbf{B}\mathbf{B}^T \tag{4}$$

where *s* is the spring constant for stiffness matrix **S** or the damping constant for damping matrix **S**, and **B** is a vector generated from the coordinate difference between the master and spring-damper nodes.

3.2 Bridge illustration and finite element model

The multi-span bridge is shown in Fig. 2, in which after a number of continuous spans (defined as *N* in the parametric study) the bridge system contains a hinge connection between two bridge girders. For the hinge connection region, the bridge girder is supported by four bearing plates on a rectangular pier. For the bridge system, the standard section of the Taiwan high-speed rail system (Ju 2012) is used in this paper. The bridge beam supports its dead weight plus an extra-mass per unit length of 18 t/m. The Young's modulus, Poisson's ratio, and mass density of the bridge girder are 3.02×10^7 kN/m², 0.15, and 2.4 t/m³, respectively. The two factors of Rayleigh damping, *α* and *β*, for the pre-stressed bridge system equal 1.2/s and 2.3×10^{-4} s, respectively, which give approximately 5% and 2.2% damping ratios at a frequencies of 2 and 5 Hz, respectively. The rail is the JIS-60-kg type supported on an upper concrete bed with a support interval of 0.625 m in the rail direction. The concrete slab system includes an upper concrete bed, a cement-asphalt layer, and a bottom concrete bed. The Young's modulus, Poisson's ratio, and mass density for the concrete bed are 2E7 kN/m², 0.15, and 2.4 T/m³, those for the cement-asphalt layer are 0.6E6 kN/m², 0.25, and 1.6 T/m³, and those for the rail are 2E8 kN/m², 0.3, and 7.85 T/m³, respectively. The Young's modulus of the surface soil is 7.5×10^4 kN/m², and more than 50 m under the ground it is 8×10^5 kN/m². Linear interpolation was applied to determine the Young's modulus between these two depths. The mass density and Poisson's ratio of the soil are 2 T/m³ and 0.48, respectively. The two factors of *α* and *β* for the soil equal 0.774/s and 3.73×10^{-4} s, respectively, which gives an approximately 2% damping ratio at frequencies of 4 Hz and 15 Hz.

The finite element model of the bridge is 1050 m long with 35 spans, as shown in Fig. 3. Rails are modeled by two-node 3D beam elements connected to the concrete slabs modeled by eight-node solid elements every 0.625 m in the *X*-direction using two spring elements (K_{rail}=spring constant=2.5E5 kN/m in *X*, *Y* and *Z* directions), and the nodes along the rails are the wheel target nodes of the train model. The nodes along the bottom surface of the concrete slabs are slave nodes controlled by the nodes of the 3D beams for the bridge girders. The simply supported bearing plates are not located on the pier center, so the rigid beam system shown in Fig. 3(c) is used to

(a) Part of the mesh for a three-span continuous bridge (the mesh for the soil is not shown, for reasons of clarity)

(b) Mesh near the rail   (c) Simulation of the simply supported end
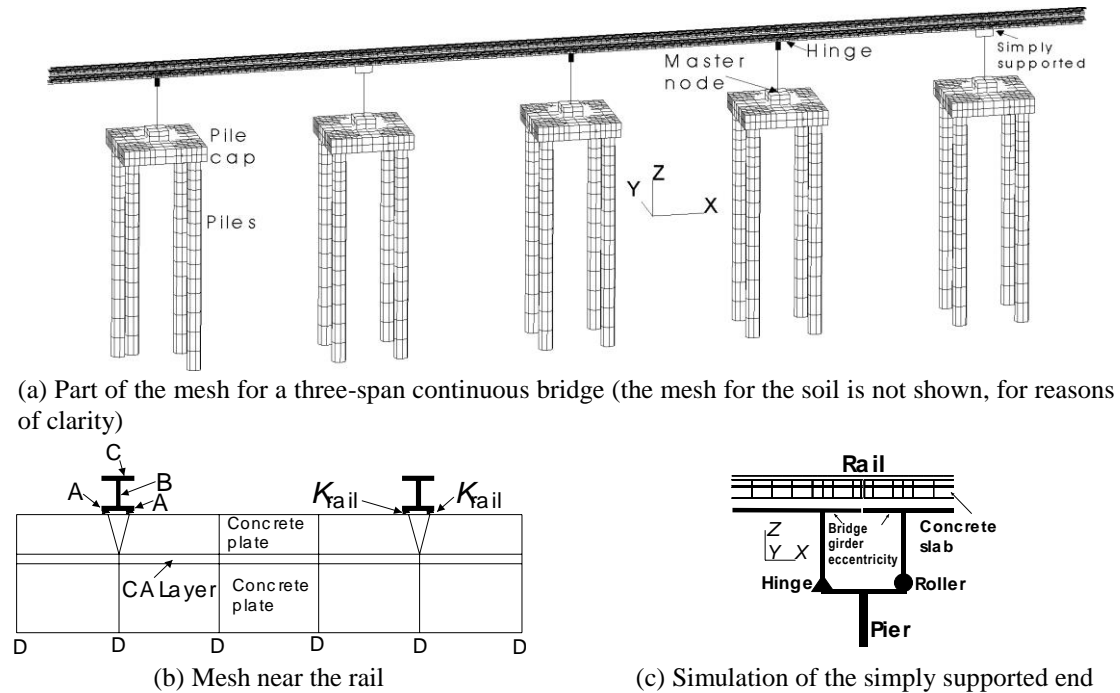
Fig. 3 Finite element mesh of a multi-span simply supported bridge (A=slave nodes that connect the beam to the concrete plate, C=slave nodes that are the target nodes of train wheels, B=rail center nodes that are the master nodes of nodes A and C, D=slave nodes that connect the concrete plate and the bridge beam center, and K_{rail}=three-direction springs)

model this eccentricity equal to 1.25m wide. The finite element model for soil and foundations is 1047 m long, 358 m wide and 139 m deep, with the maximum square element size of 2.5 m, in which the soil and bridge foundations are modeled by eight-node 3D solid elements, and the five surfaces except for the top surface of the mesh are modeled by the absorbing boundary condition (Ju and Wang 2002), Within the area of 3 m by 3 m on the center of the pile cap surface, a master-slave node scheme was used to model the connection between the pile cap (3D solid element) and the bridge column (3D beam element),

3.3 Illustration of the initial condition for soil-structure interaction analyses

The average acceleration Newmark method, Newton-Raphson method, and the consistent mass scheme are used to solve this nonlinear problem, where the time step length is 0.002 seconds, with 5,000 time steps being simulated. In the dynamic finite element analysis, the initial vertical trainloads to simulate the train gravity weight should be appropriately put into the mesh. Actually, the initial condition in realistic situation is complicated. In the numerical simulation, an equilibrium condition should be obtained first. One can perform the static analysis to find the equilibrium condition, and then do the dynamic analysis. However, complicated two steps are required, and moreover, the train speed should begin from zero. Alternative method used in this paper is to gradually apply the vertical trainloads with a large damping (10 times the normal damping) to all the mesh within the first few seconds, such as the first 1 or 2 seconds, to reduce the

initial wrong vibration. Finally, the damping is set to the correct value after this initial period.

4. Finite element results of train-induced ground vibration for multi-span bridges

This paper analyzes the vibrations using the 1/3 octave band in the frequency domain, based on an international standard in the semiconductor industry. The detailed calculations used in this method can be found in the literature (Gordon 1997, Ju 2004), First, select a time-domain velocity record (8 seconds is used in this study) to analyze using the Fast Fourier Transform, and calculate the power spectrum density function (PSDF), Then obtain the accumulated PSDF using the integration between the lower and upper band frequencies (Golden 1997), and change this to the root mean square value $\sigma_y(f_c)$ at the center frequency of f_c. Finally, obtain the frequency-dependent d_B and the total dB as follows
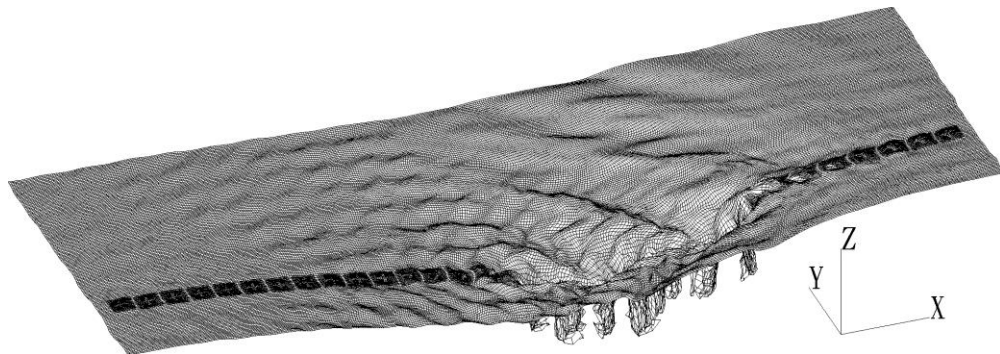
$$d_B(f_c) = 20 log_{10} \frac{\sigma_y(f_c)}{\sigma_0} \tag{5}$$

$$\text{Total } dB = 10 \times log_{10} \left(\sum_{f_c}^{\leq 100Hz} 10^{0.1 \times d_B(f_c)} \right) \tag{6}$$
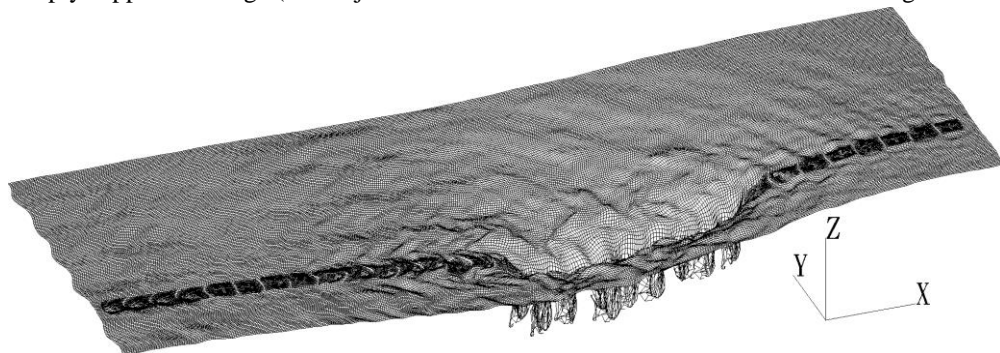
where the referred velocity $\sigma_0 = 10^{-6}$ in/sec (2.54×10^{-8} m/sec), It can be approximately estimated that an increase of 6 dB is equivalent to twice of the response. With regard to the finite element results, the central difference method is used to transform the nodal displacements to nodal velocities. The above equations can then be used to find the vibration dB.

Fig. 4 shows the surface displacements of finite element analyses with the magnifying factor of 1.5e6 under a train speed of 300 km/h for the simply supported, four-span continuous, and 12-span continuous bridges with the span length is 30 m. This figure shows the wave propagation induced by the moving train at a certain time, and it clearly indicates that the train-induced ground vibration is the largest for the simply supported bridge and the smallest for the 12-span continuous bridge, although the displacements near the bridge piers of the three cases are similar. This figure also shows that the fake reflected waves along the mesh boundaries were removed by the absorbing boundary conditions. Fig. 5 shows the vibration of the total velocity dB changing with the distance from the bridge pier for the simply supported bridge (solid line) and four-continuous-span bridge (dashed line) under a train speed of 300 km/h and a span length of 30 m. This figure indicates that the vibrations near the bridge pile are similar for the simply supported and four-span continuous bridges, while those far away from the bridge pier, such as over 50 m, are much larger for the simply supported bridge than for the four-span continuous bridge. Moreover, the difference in vibration between the two types of bridges is similar for locations more than 50 m from the bridge pier. For this reason, the rest of this study will only consider the vibrations that occur at the 50 m from the bridge. It is noted that the soil-structure interaction was included in the finite element analysis, so that the forces and moments transformed from bridge piers can be well modeled to evaluate the vibration propagation in soil.
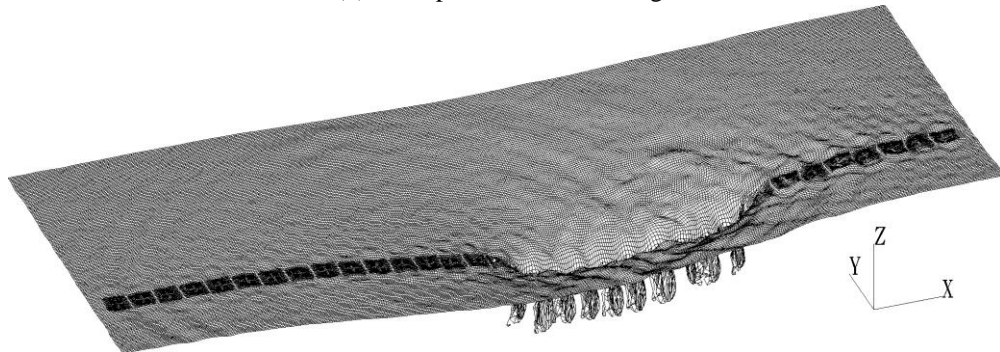
Fig. 6 shows the vibration of the total velocity dB changing with the number of continuous spans under a train speed of 300 km/h at 50 m from the bridge for the span lengths of 30 m and 35 m. The trend of the train-induced vibration decreases with an increase in the number of continuous

(a) Simply supported bridge (the major vibration is from the 5-Hz wave with a wavelength of 25 m.)

(b) four-span-continuous bridge

(c) 12-span-continuous bridge

Fig. 4 Surface displacements from the finite element analyses with the magnifying factor of 1.5e6 under a train speed of 300 km/h and a bridge span length of 30 m

spans. However, the vibration trend is uneven for the span length of 35 m, in which the vibration of the simply supported bridge can be smaller than that of four-span continuous bridge. This is because the bridge span length is around 1.4 to 1.5 times the interval of moving loads, so the vibration of the simply supported bridge under moving loads can be minimized. This condition was first mentioned by Yang *et al*. (1997), and can also be seen in Fig. 1. Nevertheless, when the number of continuous spans increases, the vibration still decreases. This figure shows the complicated vibration behavior of trains moving on bridges, and the current study will apply the bridges' natural frequencies to investigate this issue. These natural frequencies are important
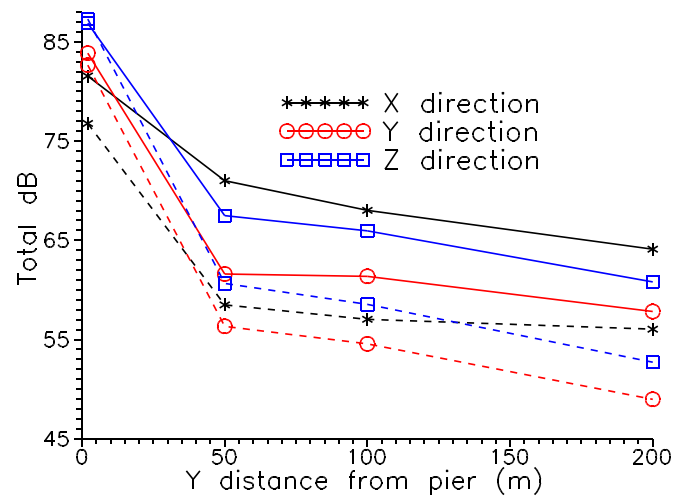
Fig. 5 Vibration of the total velocity dB changing with the distance from the bridge pier for the simply supported bridge (solid line) and four-continuous-span bridge (dashed line) under a train speed of 300 km/h

(a) Span length=30 m
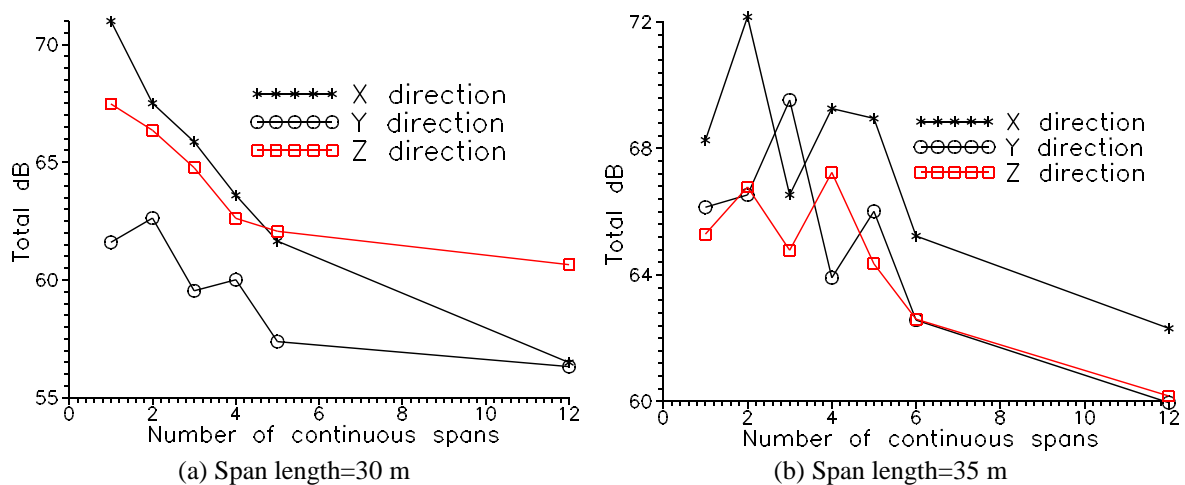

(b) Span length=35 m

Fig. 6 Vibration of the total velocity dB changing with the number of continuous spans under a train speed of 300 km/h at 50 m from the bridge

parameters that can be used to study the dynamic behaviors of structures, and the effective mass ratios are generally used to determine the major natural frequencies of structures. However, this approach is based on the dynamic equation under ground motion, and may not be suitable for trainloads; moreover, it cannot be used to compare the dynamic results between two different structures. We thus apply a comparison method based on the following dynamic finite element equation

$$\mathbf{M\ddot{X}} + \mathbf{C\dot{X}} + \mathbf{KX} = \mathbf{F} \tag{7}$$

$\mathbf{K}$, $\mathbf{C}$, $\mathbf{M}$ are finite element matrices corresponding to the stiffness, damping and mass of the

system, respectively, while **F** is the trainload vector dependent on the train speed and wheel locations. It is noted that the train mass, stiffness, and damping are neglected in the equation, and only the trainloads are considered. Using the orthogonal condition of the ith model shape vector $\mathbf{\Phi}_i$ and letting $X=\mathbf{\Phi}_i Y$, one obtains

$$\ddot{Y} + 2\xi\omega\dot{Y} + \omega^2 Y = \mathbf{\Phi}_i^{\mathrm{T}}\mathbf{F} \tag{8}$$

where ξ and ω are the damping ratio and natural frequency for this mode. We solve this equation numerically using Newmark's method to obtain the velocity field $(\dot{Y}_k, k=1,N)$ for N time steps, so that the trainloads can pass the bridge mesh. The following important factor of the ith mode shape is then calculated.

$$R_j = \sqrt{\left(\mathbf{I}_j\mathbf{\Phi}_i\right)\cdot\left(\mathbf{I}_j\mathbf{\Phi}_i\right)\frac{1}{N}\sum_{k=1}^{N}\dot{Y}_k^2} \quad , j\text{=}x, y, \text{ or } z \tag{9}$$

where $\mathbf{I}_j$ is a diagonal matrix whose diagonal component is one if the degree of freedom in a certain region is active in the j direction, and zero otherwise. The current study chooses the nodes at the bottom of bridge piers to find R_j in order to examine the important factor of this mode shape.

The natural frequencies of the cases in Fig. 6 were first obtained before Eq. (9) was applied. In this figure the superstructure is the same as that in Fig. 3, but the foundation and soil are modeled using a six-degree-of-freedom equivalent spring (Ju 2002). In this way the number of the degrees of freedom in the related eigenproblem can be significantly reduced. Eq. (9) is then used to find the important factor in the Z direction of each mode, and the results are shown in Fig. 7 for the simply supported and four-span continuous bridges with bridge spans of 30 m and 35m. Two observations are made about this figure: (1) With a bridge span length of 30 m, the vibration of the simply supported bridge is larger than that of the four-span continuous bridge, and with a bridge span of 35 m this condition is reversed. This phenomenon, as shown in Fig. 6, can be clearly seen in Fig. 7, in which the magnitude distribution of the important factor R_j is consistent with this

(a) Bridge span length=30 m   (b) Bridge span length=35 m
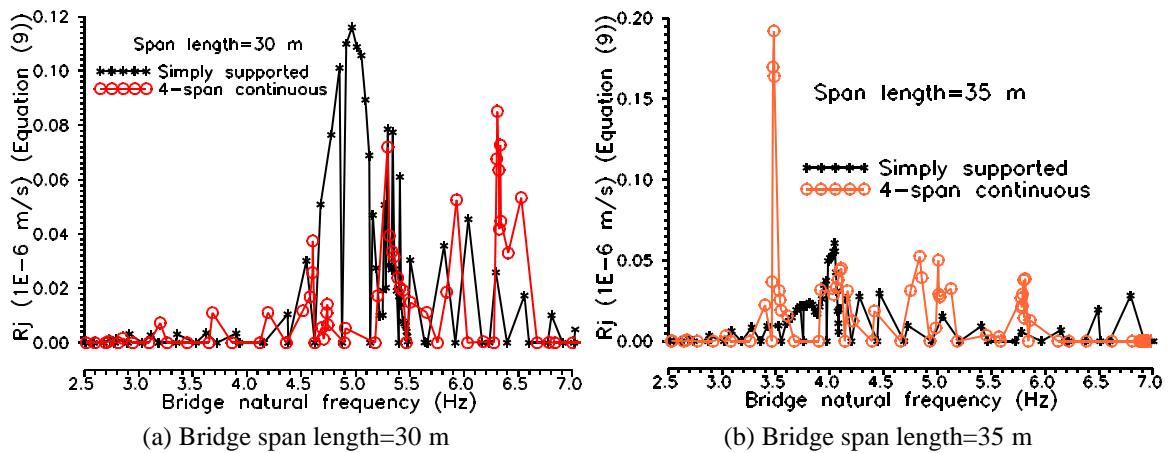
Fig. 7 Important factor (Eq. (9)) in the Z direction of each mode for the simply supported and four-span continuous bridges with the bridge spans of 30 m and 35 m
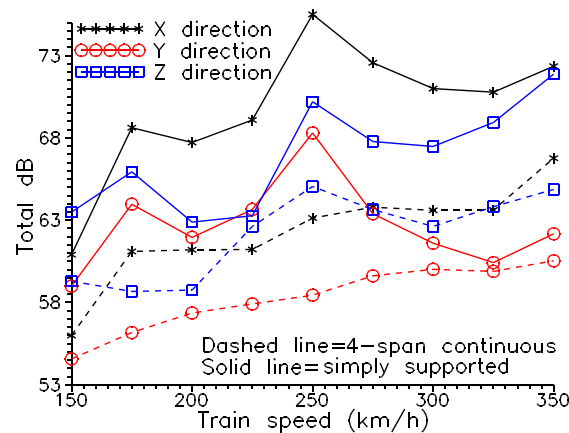
Fig. 8 Vibration of the total velocity dB changing with the train speed at 50 m from the bridge pier

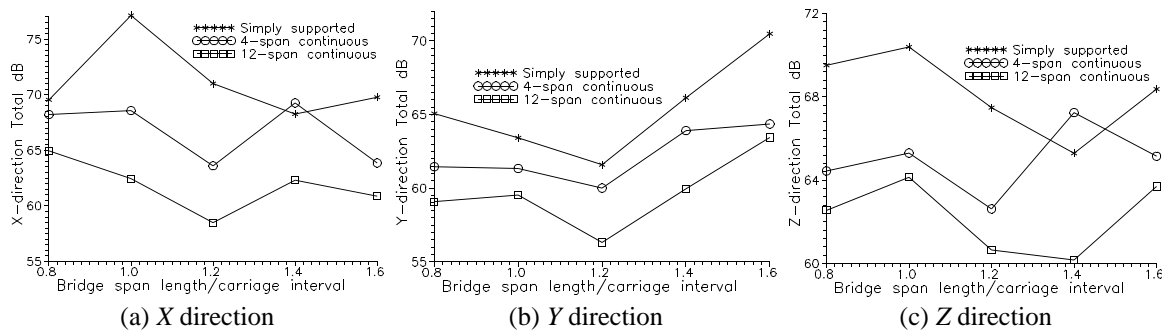(a) *X* direction   (b) *Y* direction   (c) *Z* direction

Fig. 9 Vibration of the total velocity dB changing with the normalized span length under a train speed of 300 km/h at 50 m from the bridge pier

observation. (2) For the simply supported bridge with a span length of 30 m, the bridge's natural frequency of about 5 Hz produces a large vibration. This condition can be clearly observed in Fig. 4(a), where the major vibration is from the 5-Hz wave with the wavelength of 25 m.

The train speed (*V*) will change the dominant frequencies (*nV/D*) of the trainloads, so that these dominant frequencies become close to the bridge's natural frequencies, and thus produce resonance. Therefore, the simply supported and four-span continuous bridges with a span length of 30 m were analyzed under a train speed ranging from 150 to 350 km/h. Fig. 8 shows the vibration of the total velocity dB changing with the train speed. This figure indicates that the ground vibrations of the simply supported bridge in the three directions are always larger than those of the four-span continuous bridge. The *Z*-direction vibrations of the two types of bridges are similar for the train speed of 225 km/h, and their *Y*-direction vibrations are similar for the train speed of 325 km/h. Fig. 9 shows the vibration of the total velocity dB changing with the ratio of the bridge span length over the train carriage interval at the train speed of 300 km/h. This figure indicates that the vibrations of 12-span continuous bridges are always smaller than those of other two types. Except for when the simply supported bridge has an optimal ratio (1.4 to 1.5) of bridge span length to train carriage interval, the vibrations of simply supported bridges are always larger than those of four-span continuous bridges. Since the train usually operates at a constant speed, the finite element analyses are suggested to be performed with this constant train speed in order to find the
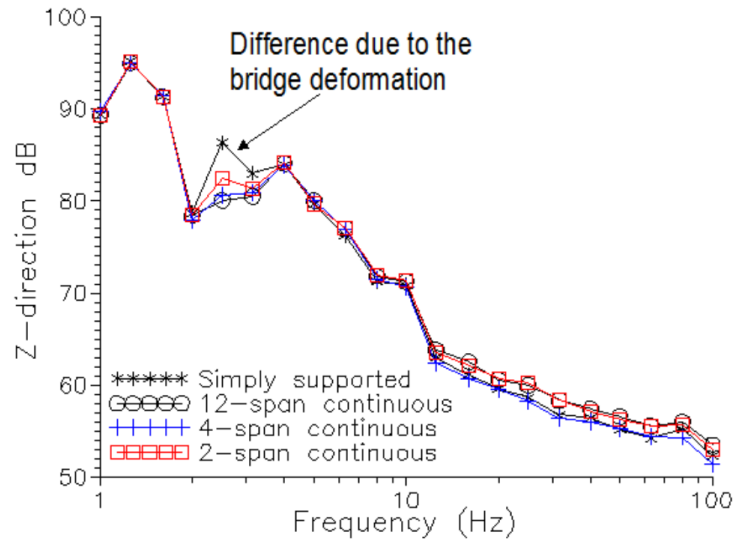
Fig. 10 Vertical vibration of the velocity dB at the center of the first carriage under a train speed of 300 km/h

most suitable type of bridge to reduce the amount of ground vibration.

Vibration in moving trains passing multi-span bridges is also studied in this section. Fig. 10 shows the velocity dB in the center of the first carriage. This figure indicates that the vibration in the train is almost independent of the bridge types. The only obvious difference near the frequency of 2.8 Hz is due to the vertical deflection of the bridge girders, while each train carriage passes them with the frequency of V/L Hz (2.8 Hz=83.3(m/s)/30(m), where V=train speed and L=bridge span length), Thus, the major part of the vibration in the train is generated from the rail irregularities, and that from the bridge is often not dominant. It is noted that the rail irregularities used from Ju (2012) are considerably smooth and have an amplitude of 2 mm per 20 m of the rail in the vertical and transverse directions of the rail, which is the standard rail irregularities in the Taiwan high-speed rail system.

5. Conclusions

(1) The dynamic impact factor of multi-span continuous bridges under train loads was determined in this work to better examine the vibration behaviors of these structures. The results of a parametric study show that the dynamic impact factor will be large when the first bridge vertical natural frequency is equal to nV/D, and this condition is especially apparent when n=1. This is because a resonance occurs at this condition, and this resonance is more serious for a smaller ratio of the bridge span over the trainload interval (L/D). The trainload interval is usually constant, so resonance, particularly with the first trainload dominant frequency, should be avoided for a short bridge span. In addition, more continuous spans will produce smaller dynamic impact factors at the resonance conditions. While it is difficult to build bridges with too many continuous spans, since the changes in temperature may cause mechanical problems, four or five continuous spans are still feasible for bridge systems.

(2) This paper developed nonlinear time-domain finite element procedures using the

soil-structure interaction in order to analyze the wave propagation that occurs when high-speed trains cross bridges. Although most of the finite elements considered in this work, such as the nonlinear wheel element, spring-damper elements, rigid links, and absorbing boundary conditions, were also used in previous studies, this work is the first to combine them to perform a time-domain nonlinear finite element analyses with about ten million degrees of freedom. Since trains usually operate at a constant speed, it is suggested that the vibration finite element analyses be carried out at this constant train speed in order to find the type of bridge that can best reduce ground vibration.

(3) For realistic high-speed rail bridges, the 3D finite element results show that the trend of the train-induced vibration decreases as the number of continuous spans increases. However, when the bridge span length is about 1.4 to 1.5 times that of the carriage interval, the vibration of the simply supported bridge under moving loads can be minimized, so that the change in the vibration trend along with the number of continuous spans is uneven, and simply supported bridges can have better performance with regard to reducing train-induced vibration than two- to four-span continuous bridges. It is thus suggested that the bridge span be set at 1.4 to 1.5 times the carriage interval for simply supported bridges, and if not, then it is recommended that four- or more-than-four-span continuous bridges be used to reduce train-induced vibration. This paper also indicates that the vibration in the train is almost independent of the bridge types, and the major part is generated from the rail irregularities, so maintaining a smooth rail should be one of the best ways to reduce vibration in the train.

References

Adam, C. and Salcher, P. (2014), "Dynamic effect of high-speed trains on simple bridge structures", *Struct. Eng. Mech.*, **51**(4), 581-599.

Aflatooni, M., Chan, T.H.T. and Thambiratnam, D.P. (2015), "A new look at the restrictions on the speed and magnitude of train loads for bridge management", *Struct. Eng. Mech.*, **53**(1), 89-104.

Arvidsson, T., Karoumi, R. and Pacoste, C. (2014), "Statistical screening of modelling alternatives in train-bridge interaction systems", *Eng. Struct.*, **59**, 693-701.

Fiebig, W. (2010), "Reduction of vibrations of pedestrian bridges using tuned mass dampers (TMD)", *Arch. Acoust.*, **35**, 165-174.

Gordon, C.G. (1997), "Generic vibration criteria for vibration-sensitive equipment. optics and metrology", **1619**, 71-75.

Ju, S.H. (2002), "Finite element analyses of wave propagations due to a high-speed train across bridges", *Int. J. Numer. Meth. Eng.*, **54**, 1391-1408.

Ju, S.H. (2004), "Three-dimensional analyses of wave barriers for reduction of train-induced vibrations", *J. Geotech. Geoenviron. Eng.*, **130**, 740-748.

Ju, S.H. (2012), "Nonlinear analysis of high-speed trains moving on bridges during earthquakes", *J. Nonlin. Dyn.*, **69**, 173-183.

Ju, S.H. (2013), "Improvement of bridge structures to increase the safety of moving trains during earthquakes", *Eng. Struct.*, **56**, 501-508.

Ju, S.H., Lin, H.T. and Huang, J.Y. (2009), "Dominant frequencies of train-induced vibrations", *J. Sound Vib.*, **319**, 247-259.

Kim, C.W., Kawatani, M. and Hwang, W.S. (2004), "Reduction of traffic-induced vibration of two-girder steel bridge seated on elastomeric bearings", *Eng. Struct.*, **26**, 2185-2195.

Kim, S.I. and Kim, N.S. (2010), "Dynamic performances of a railway bridge under moving train load using experimental modal parameters", *Int. J. Struct. Stab. Dyn.*, **10**, 91-109.

Kwark, J.W., Chin, W.J., Cho, J.R., Lee, J.W., Kim, B.S. and Lee, K.C. (2012), "Vibration reduction for a

high-speed railway bridge in South Korea", *Proceedings of the Institution of Mechanical Engineers Part F-Journal of Rail and Rapid Transit*, **226**, 174-186.

Lavado, J., Domenech, A. and Martinez-Rodrigo, M.D. (2014), "Dynamic performance of existing high-speed railway bridges under resonant conditions following a retrofit with fluid viscous dampers supported on clamped auxiliary beams", *Eng. Struct.*, **59**, 355-374.

Mao, L. and Lu, Y. (2013), "Critical speed and resonance criteria of railway bridge response to moving trains", *J. Bridge Eng.*, **18**, 131-141.

Museros, P. and Martinez-Rodrigo, M.D. (2007), "Vibration control of simply supported beams under moving loads using fluid viscous dampers", *J. Sound Vib.*, **300**, 292-315.

Wang, Y., Wei, Q., Shi, J. and Long, X. (2010), "Resonance characteristics of two-span continuous beam under moving high speed trains", *Latin Am. J. Solid. Struct.*, **7**, 185-199.

Wang, Y.J., Wei, Q.C. and Yau, J.D. (2013), "Interaction response of train loads moving over a two-span continuous beam", *Int. J. Struct. Stab. Dyn.*, **13**(1), No:1350002.

Xia, H., Chen, J.G., Xia, C.Y., Inoue, H., Zenda, Y. and Qi, L. (2010), "An experimental study of train-induced structural and environmental vibrations of a rail transit elevated bridge with ladder tracks", *Proceedings of the Institution of Mechanical Engineers Part F-Journal of Rail and Rapid Transit*, **224**, 115-124.

Xin, T. and Gao, L. (2011), "Reducing slab track vibration into bridge using elastic materials in high speed railway", *J. Sound Vib.*, **330**, 2237-2248.

Yang, Y.B., Lin, C.L., Yau, J.D. and Chang, D.W. (2004), "Mechanism of resonance and cancellation for train-induced vibrations on bridges with elastic bearings", *J. Sound Vib.*, **269**, 345-360.

Yang, Y.B., Yau, J.D. and Hsu, L.C. (1997), "Vibration of simple beams due to trains moving at high speeds", *Eng. Struct.*, **19**(11), 936-944.

CC